

Oscillons in the presence of external potential

Tomasz Romańczukiewicz^a Yakov Shnir^{b,c,d}

^a*Institute of Physics, Jagiellonian University,
Lojasiewicza 11, 30-348 Kraków, Poland*

^b*BLTP, JINR,
Dubna 141980, Moscow Region, Russia*

^c*Department of Theoretical Physics and Astrophysics,BSU,
Minsk 220004, Belarus*

^d*Department of Theoretical Physics, Tomsk State Pedagogical University,
Russia*

E-mail: trom@th.if.uj.edu.pl, shnir@maths.tcd.ie

ABSTRACT: We discuss similarity between oscillons and oscillational mode in perturbed ϕ^4 . For small depths of the perturbing potential it is difficult to distinguish between oscillons and the mode in moderately long time evolution, moreover one can transform one into the other by adiabatically switching on and off the potential. Basins of attraction are presented in the parameter space describing the potential and initial conditions.

KEYWORDS: Field Theories in Lower Dimensions, Nonperturbative Effects, Solitons Monopoles and Instantons

Contents

1	Introduction	1
2	The model	3
2.1	Definition and static solutions	3
2.1.1	Sector $\phi = 1$	4
2.1.2	Sector $\phi = -1$	4
2.2	Linear stability of static solutions	6
2.3	Radiative decay of the oscillational modes	8
2.4	Oscillons	9
3	Numerical Results	10
3.1	Numerical methods	10
3.2	Oscillon and mode evolution	10
3.3	Adiabatic transformation	11
3.4	Final state	12
3.5	Phase diagram	14
4	Conclusions	15
A	Time evolution of the oscillational mode	18
A.1	Manton-Merabet power law	18
A.2	Numerical verification	19
A.3	Deep modes relaxation	21

1 Introduction

In the field theory the long time evolution of a dynamical system is usually governed by the spectral structure of small perturbations around the static solution, such as for example a soliton. There the eigenmodes of the corresponding linearized problem play very important role. Usually there is a continuous spectrum of scattering modes and a discrete sequence of oscillational (normal) modes. The lowest mode of the continuum is often referred to as the mass threshold.

The resonance states, or quasinormal modes also play quite important role in the long time dynamics of the system. They are defined as the solution of the linearized system which corresponds to the purely outgoing wave, they can also be defined as the complex poles of the Green function. Thus, their eigenfrequencies are complex valued, the imaginary part of them is responsible for exponential decay of the corresponding mode. Usually the

mode with the lowest damping is the one which is seen in the late time dynamics, it is the most long living.

Recall that in the linear system the normal modes, which have real frequencies, live infinitely long. However, in nonlinear theories these modes are coupled to the states of the continuum spectrum. In the case of the quadratic non-linearity such a coupling yields an outgoing wave which has twice the frequency of the oscillational normal mode. Such a wave carries away the energy and causes the oscillational mode to decay. As shown in [1, 2], this results in the decay of the discrete mode amplitude according to the power law, $A \sim t^{-1/2}$.

However, if the oscillational mode has a low frequency, even the corresponding second harmonic may still be below the mass threshold and therefore it cannot propagate. Then only the higher harmonics can carry away the energy. This possibility was firstly described in [3].

Note that the nonlinearities also can lower the frequency of the oscillational mode when it is highly excited. However, when its amplitude is decreasing, the corresponding frequency tends to the value one can find from the linearized problem.

Usually, the scattering modes of the continuous spectrum quickly radiate the energy away (except the quasinormal resonance modes) and do not play any role in the long time evolution of the system. However, there is yet another exception. Recall that the speed of propagation of waves in massive field theories depends on the frequency. The slowest modes are the ones which are near the mass threshold when the propagation frequency tends to zero. As a result the generic initial conditions may develop slowly decaying field with the frequency of the threshold. As was shown for example in [4] this oscillations decay as $t^{-1/2}$ or, when a resonance is on the threshold, as $t^{-2/3}$.

Peculiar feature of many non-linear models is that they also support time dependent non-perturbative soliton-like solutions which are not captured by the linear analysis. The well know example is the breather configuration in the 1+1 dimensional sine-Gordon model. It is an exact periodic solution to the nonlinear equation which does not lose its energy into radiation, so it has an infinite lifetime. However, sine-Gordon model is exceptional since it is integrable and the states of the continuum are completely separated from the solutions of the field equations. On the other hand, in non-integrable models, like ϕ^4 theory, such a breather-like configuration with finite energy cannot exist infinitely long ¹ because they decay radiating small amount of energy away [6].

However, in the ϕ^4 model there are quasi-non-dissipative and almost periodic time-dependent configuration, the oscillons [7–9]. They appear as quasi-breathers, which are localised, extremely long-lived regular finite energy configurations performing non-harmonic oscillations about the one of the vacua. Typically, the radiation energy of the oscillon is extremely small, numerical simulations reveal that in 1+1 dimensions the oscillon survives after a few millions of oscillations [10, 11] with the decay rate $dE/dt \sim -\exp(-B/E)$ beyond all orders [6].

¹The model with V-shaped potential [5] may support non-radiating time-periodic compacton solution, which is an exception.

The interplay between the states of the perturbative spectrum of the ϕ^4 theory and solitons, kinks and oscillons, attracted a lot of attention. The most familiar observation is the resonance effect observed in the bouncing collisions of the kink–anti-kink ($\bar{K}K$) pair and excitation of the internal vibrational mode of the kink [12, 13].

It was pointed out that the excitations of the internal mode of the kink may produce kink–anti-kink pairs [1]. In [14] it was shown that such mode can be excited by radiation via parametric resonance leading to the defect production. The kink–anti-kink pair can also be produced in the absence of a single soliton via the resonance excitations of the oscillon by the incoming waves [15] showing another resemblance between oscillons and oscillational modes.

In the present paper we will show that there is also a correspondence between the internal mode of the external potential and the oscillon, which under special conditions, can smoothly be transferred into each other.

2 The model

2.1 Definition and static solutions

We consider the standard one-dimensional ϕ^4 model with an additional external potential $V(x)$ defined by Lagrangian density

$$\mathcal{L} = \frac{1}{2}\phi_t^2 - \frac{1}{2}\phi_x^2 - \frac{1}{2}(\phi^2 - 1)^2 - \frac{1}{2}V(x)(\phi - 1)^2 \quad (2.1)$$

As the perturbation potential we have chosen the Pöschl-Teller potential

$$V(x) = -\frac{V_0}{\cosh^2 bx} \quad (2.2)$$

since it is vanishing asymptotically and all solutions of the corresponding eigenvalue problem are known analytically. Because oscillons are symmetric we limit our considerations only to even symmetry $\phi(-x) = \phi(x)$.

Physically, such a trapping potential corresponds to a localized inhomogeneity (impurity), similar impurity potential was introduced in the sine-Gordon models to investigate the effects of inhomogeneities in the kink-antikink scattering process [16, 17]. In the limiting case of a localized impurity at the origin, the defect corresponds to a delta-function, such a potential was used in the ϕ^4 model to study kink-impurity interactions [18], further investigation reveal very interesting pattern of resonance scattering of the kinks on the impurities [17].

The static solutions obey the time-independent equation

$$\phi_{xx} = 2\phi(\phi^2 - 1) + V(x)(\phi - 1). \quad (2.3)$$

For even symmetry the solutions has no topological charge $\phi(-\infty) = \phi(\infty) = \phi_v$, where $\phi_v = \pm 1$ is one of the usual ϕ^4 vacuum. The second condition is $\phi_x(0) = 0$. These conditions, however, do not define unique solutions.

2.1.1 Sector $\phi = 1$

In the topological sector with $\phi_v = 1$ there are two solutions. First one is the trivial vacuum $\phi \equiv 1$, clearly this is zero energy state.

There is yet another solution in this sector, which for small values of V_0 resembles an antikink–kink pair ($\bar{K}K$)

$$\phi(x) \approx \tanh(x - X) - \tanh(x + X) + 1. \quad (2.4)$$

Energy of such configuration for $b = 1$, relatively small values of V_0 and large values of X , can be found approximately

$$E \approx 2M - 16e^{-4X} - 2\pi V_0 (1 - 2e^{-X}), \quad (2.5)$$

where $M = 4/3$ is a mass of a single kink. This is the usual Yukawa interaction between the well separated kink antikink pair, modulated by the perturbation potential. Since the Yukawa interaction is attractive, the solution of that type cannot exist in the absence of the external potential, nor for $V_0 < 0$ when the potential also becomes attractive.

However, for $V_0 > 0$ the energy for $\bar{K}K$ has a maximum for

$$X = -\frac{1}{3} \log \left(\frac{\pi V_0}{16} \right). \quad (2.6)$$

Thus, the pair $\bar{K}K$ can be held together by the external potential, however, small perturbation can destabilize the configuration as it is the maximum of energy and the pair can either separate or collapse and annihilate. As V_0 increases the approximation (2.4) is no longer valid and the shape of the solution becomes a lump centered at $x = 0$ vanishing for $V_0 = 6$. Energy of this solution decreases from the energy of two static kinks as $V_0 = 0$: $E(0) = 2M = 8/3$ to 0 as $V_0 = 6$. In Fig. 1 we display some example of corresponding profiles for some set of values of V_0 . For very small value of $V_0 = 5 \cdot 10^{-5}$ we can evaluate the separation between the kinks from the equation (2.5), it is equal to $X = 3.84$ which seems to be just little less then the value obtained from the solution of the corresponding static equation.

2.1.2 Sector $\phi = -1$

Note that unlike the original ϕ^4 model, the model (2.1) has only one trivial solution $\phi = 1$. In the second topological sector the static configuration, which asymptotically tends to $\phi = -1$ as $x \pm \infty$, is a nontrivial solution localized by the potential (2.2). It is similar to a non-topological soliton (lump), which appears in the two-component system of coupled fields [19, 20]. However, in the model (2.1) the lump centered at $x = 0$ is trapped by the potential $V(x)$, it cannot propagate.

Although we have not found this solution analytically, one can easily find it numerically, in Fig. 2 we plotted the corresponding profiles of the vacuum configurations at $b = 1$ and a few values of the parameter V_0 . As V_0 is positive, $\phi(0) < -1$, for negative values of the parameter V_0 the value of the field at the center of the trapping potential is $\phi(0) > -1$.

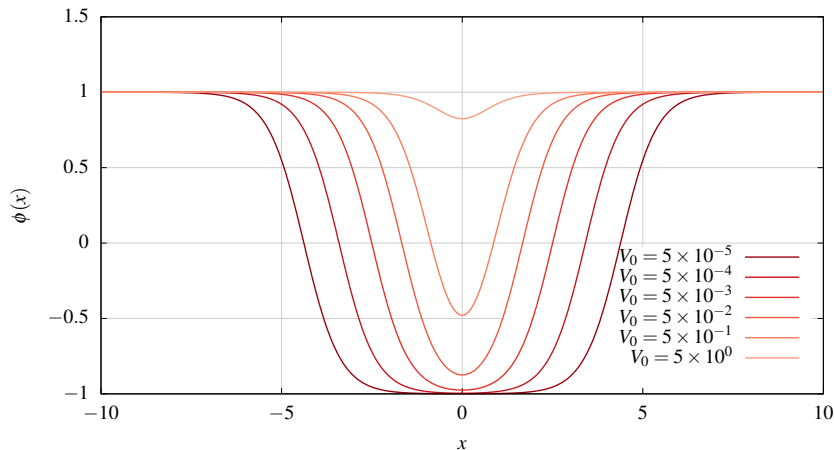


Figure 1. Static (unstable) $\bar{K}K$ solutions in the topologically trivial sector.

The energy of the lump is set to be zero as $V_0 = 0$, it is positive for negative values of V_0 and it is negative as $V_0 > 0$ decreasing monotonically as V_0 increases.

Again, as in the first sector, we have found another solution, which represents a static kink-antikink pair, captured by the potential

$$\phi(x) \approx \tanh(x + X) - \tanh(x - X) - 1. \quad (2.7)$$

The energy of this configuration, for large value of X and small V_0 can be found as

$$E \approx 2M - 16e^{-4X} - 4\pi V_0 e^{-X}. \quad (2.8)$$

The above energy has maximum for

$$X = -\frac{1}{3} \log \left(-\frac{\pi V_0}{16} \right). \quad (2.9)$$

is just above the total mass of two static ϕ^4 kinks, $E \approx 2M = 8/3$. Clearly this solution is unstable, it can decay into the vacuum $\phi = 1$ with two kinks escaping to infinity or into the lump solution which is in the same topological sector but has less energy.

The stable lump solution and a single example of the unstable $K\bar{K}$ solution are shown in Figure 2.

The energies of the four static solutions are gathered in the Figure 3. Note that the energy of a lump increases as V_0 decreases. For $V_0 < -0.761$ the energy of the lump is larger than the energy of the unstable $K\bar{K}$. This means that the system has no stable solution in the sector $\phi(|x| \rightarrow \infty) = -1$, it always decays to the $\phi = 1$ solution emitting a kink-antikink pair.

For $V_0 > 0$ the lump solution has lower energy than the stable solution in the first topological sector, $\phi = 1$. However, for $V_0 < 6$ the system cannot jump spontaneously from $\phi = 1$ to the lump solution emitting the kink-antikink pair because of the energy threshold. The minimal energy which allows such a transition is defined by the mass of the

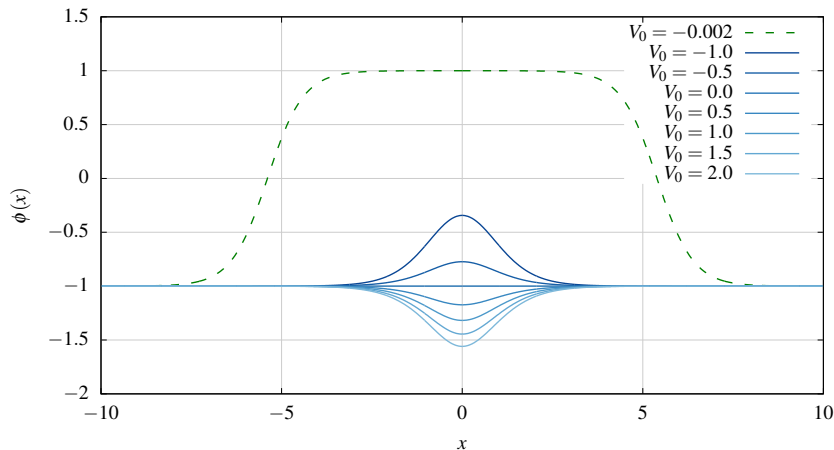


Figure 2. Static lump solutions of the model (2.1) with the potential (2.2) at $b = 1$ for a few different values of V_0 .

static $\bar{K}K$ configuration. Note the energy difference between the lump solution and the pair $\bar{K}K$, quickly increases as V_0 grows. Hence the velocity of the emitted pair of kinks also increases.

In the rest of the paper we will consider the excitations of the solution in the sector $\phi = 1$. So the process of $\bar{K}K$ emission would be more and more possible as V_0 grows and the energy threshold decreases to 0 for $V_0 = 6$.

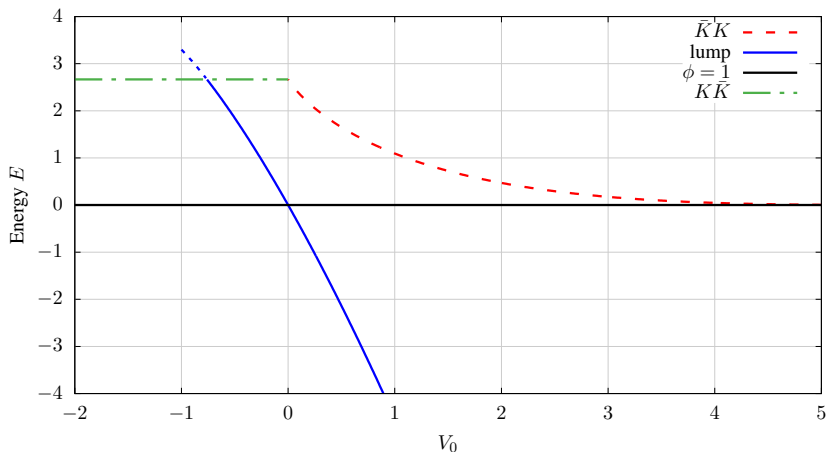


Figure 3. Energies of the static solutions of the model (2.1) vs V_0 . Dashed curves correspond to the unstable solutions, see Figs. 1 and 2

2.2 Linear stability of static solutions

Generally, solutions of a nonlinear field theoretical model can be decomposed into the infinitely many modes oscillating with different frequencies. However, our study focuses on some special solutions which are almost periodic. Such a period defines the basic frequency

of the solution, which we would refer to as the frequency. The power spectrum then usually consists of the basic frequency along with the higher harmonics, which, due to nonlinearity, are often contaminated via excitations of other modes. During the time evolution the basic frequency may change, typically the corresponding time interval is much larger than the period of the solution. On the other hand, we can consider linearized equations of motion, in such a case the frequency of the corresponding oscillational modes, would be referred to as the linearized frequency or eigenfrequency.

Let us consider the linearized fluctuations around the trivial vacuum $\phi = 1 + e^{i\omega t}\eta(x) + c.c.$ in the model (2.1). The corresponding eigenfunctions are solutions of the equation

$$-\eta_{xx} + (m^2 + V(x))\eta = \omega^2\eta. \quad (2.10)$$

where $m = 2$ is the mass of the mode. The potential (2.2) yields the ground state

$$\eta_0(x) = \frac{1}{\cosh^\lambda(bx)}, \quad \lambda(\lambda + 1) = \frac{V_0}{b^2}, \quad \omega^2 = m^2 - b^2\lambda^2 \quad (2.11)$$

where λ is a real parameter. Recall that in the particular case when λ is an integer, the Pöschl-Teller potential is reflectionless.

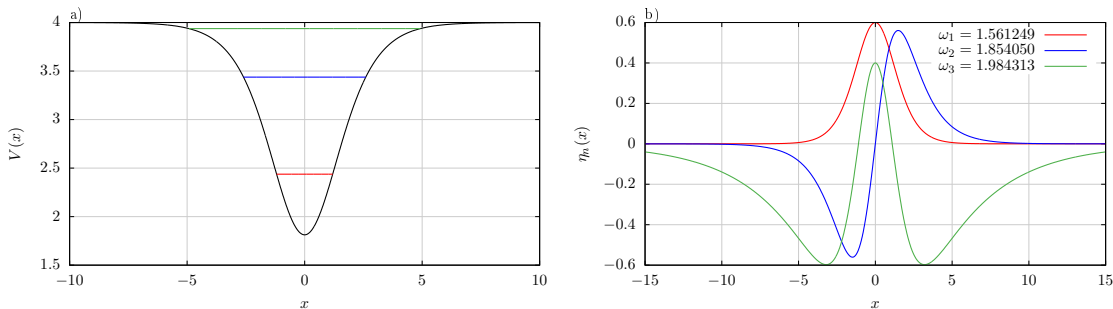


Figure 4. Example potential (a) and the profiles of the bound states (b) for $b = 0.5$, $\lambda = 2.5$ and $V_0 = 2.1875$.

The equation for λ has exactly one positive solution for $V_0 > 0$. For $V_0 > 4 + 2b$ the eigenfrequency of the ground state becomes imaginary, i.e. $\omega^2 < 0$ (Figure 5). It means that the corresponding mode is unstable and the system could change its ground state producing kink–anti-kink pair. Further, one can expect that in the presence of the perturbation potential, the lowest oscillational mode could become an attractor in the time evolution of some even initial data, which, in the limit $V_0 = 0$ would evolve into the oscillon-like state. For $b < 1$ there can be more eigensolutions, frequencies of which are given by

$$\omega_j^2 = m^2 - b^2(\lambda - j)^2, \quad 0 \leq j < \lambda. \quad (2.12)$$

Similar analysis around the second solution, which asymptotically approaches the vacuum $\phi = -1$ as $x \rightarrow \pm\infty$, shows that there are no oscillational modes for $b = 1$ and $V_0 < 0$. The corresponding effective potential, which appears in the linearized equation for excitations

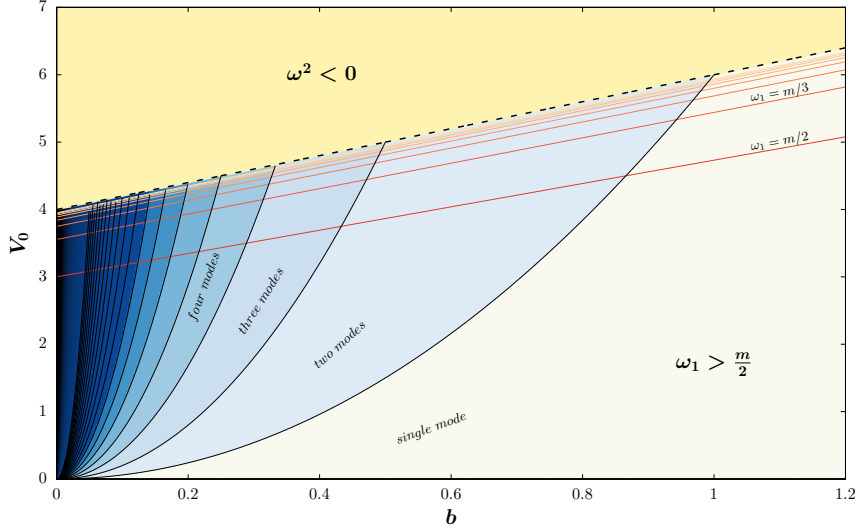


Figure 5. Spectral structure of even solutions of Pöschl-Teller potential. Red and orange lines correspond to values where the frequency of the first mode is equal to m/n for integer $n \geq 2$.

is

$$V_{eff}(x) = 6\phi_s^2(x) - 2 + V(x), \quad (2.13)$$

it is repulsive for $V_0 < 0$. $\phi_s^2(x)$ is the static solution. Below we mainly restrict our consideration to the case of fluctuations about the trivial vacuum $\phi_v = 1$.

2.3 Radiative decay of the oscillational modes

In nonlinear theories the oscillational modes are coupled to the higher frequency modes from the continuous spectrum. These higher modes can propagate radiating away the energy, initially stored in the oscillational modes, and causing their decay. In particular, it has been shown that the rate, at which the oscillational mode of the ϕ^4 kink decays, obeys the power law [1]

$$A(t) \sim t^{-1/2}. \quad (2.14)$$

In the Appendix we show that the similar law can be applied to the shallow oscillational modes of the external potential in the model (2.1). Note that there is a single oscillational mode of the ϕ^4 kink configuration, it decayed via radiation propagating through the second harmonic. On the other hand, the model (2.1) may also support higher oscillational modes with eigenfrequencies below $m/2$ for which the second harmonic cannot propagate because it is below the mass threshold. In such a case the decay is caused by at least the third harmonic generated in the third order of the perturbation scheme. This leads to the different character of the decay. In the Appendix we provide more details of the process of decay of the higher oscillational modes in the model (2.1) and discuss the dynamical transitions between different scenarios.

Throughout the paper (except the Appendix) we will restrict our considerations to the case of $V_0 < 2$, this corresponds to the oscillational modes with frequencies well above the threshold $m/2$, above which the second harmonics can propagate.

As the oscillational mode is excited to a nonlinear regime, its frequency becomes lowered and the profile becomes more narrow. Evolving in time, such a mode radiates some amount of energy, so its amplitude decreases according to the Manton-Merabet rule $A \sim t^{-1/2}$ [1]. The frequency of this mode increases with time, its profile becomes broader as the mode evolves toward the linear regime.

2.4 Oscillons

The lifetime of the oscillons is very large, so they can be well approximated by the Fourier decomposition

$$\phi(x, t) = 1 + \sum_{n=0}^N \phi_n(x) \cos(n\omega t). \quad (2.15)$$

Note that such a periodic solution with the frequency $\omega < m$ cannot have a finite energy². We can consider the pseudobreathers, which are the corresponding oscillating solutions, which minimize the oscillatory tails. Such tails represent a standing wave which can be considered as a superposition of two waves, propagating in opposite directions. One of these waves can be considered as the radiation, which carries away the energy, whereas the other incoming wave stabilizes the pseudobreather.

However, the physical oscillons possess only outgoing radiation tails. During the evolution the amplitude of the oscillon slowly decreases, and the rate, in which it radiates, decreases even faster. Therefore oscillons live exceptionally long and the decay rate is beyond all orders [6]

$$\frac{dE}{dt} \sim \exp(-B/E). \quad (2.16)$$

In the unperturbed 1+1 dimensional ϕ^4 the oscillons tend to the lowest mode of the continuous spectrum at $\omega = m$. As it was shown in [6, 21], the ϕ^4 model can be treated as a perturbation to the sine-Gordon model

$$u_{tt} - u_{xx} + \sin u = 0, \quad (2.17)$$

which exhibits exact, periodic solutions called the breathers

$$u(x, t) = 4 \arctan \left[\frac{\sqrt{1 - \omega^2}}{\omega} \frac{\cos(\omega t)}{\cosh(\sqrt{1 - \omega^2} x)} \right]. \quad (2.18)$$

To match the expansion of the sG equation with the ϕ^4 equation around $\phi = 1$ one has to rescale the variables $(x, t, \omega)_{sG} \rightarrow (2x, 2t, \omega/2)_{\phi^4}$. It is conjectured that the first approximation to the oscillon can be written as a rescaled breather

$$\phi(x, t) \approx 1 + 4 \arctan \left[\frac{\sqrt{1 - \omega^2/4}}{\omega/2} \frac{\cos(\omega t)}{\cosh(2\sqrt{1 - \omega^2/4} x)} \right] \quad (2.19)$$

²The sine-Gordon breathers, which are solutions of the integrable model, are exceptions.

which should be valid for low amplitude oscillons. Defining the new variable

$$\epsilon = 2\sqrt{1 - \omega^2/4} \quad (2.20)$$

the lowest approximation of their profiles in ϕ^4 can be nicely described as

$$\phi_1(x) = 2\epsilon \operatorname{sech}(\epsilon x), \quad (2.21)$$

which oscillates with the frequency $\omega = 2\sqrt{1 - \epsilon^2/4}$. Other profiles and the correction to the profile of ϕ_1 are of order $\mathcal{O}(\epsilon^2)$. It is worth mentioning that (2.21) is not a solution of any linearized equation and higher order corrections (even though much smaller than ϕ_1) are essential to stabilize the solution.

3 Numerical Results

3.1 Numerical methods

To solve the equation of motion following from the Lagrangian (2.1) we applied the method of lines using five point stencil to approximate the spatial derivative and fourth order symplectic method to integrate in time. Typically the space grid was $\delta x = 0.05$ and time step $\delta t = 0.4\delta x$, but we change the values to ensure stability and convergence of the solutions. At $x = 0$ we imposed symmetric boundary conditions $\phi(-x) = \phi(x)$. The second boundary was chosen in such distance (more than half of the evolution time) so that the waves had no time to reflect and come back to interfere with the field at $x = 0$.

3.2 Oscillon and mode evolution

The results of the numerical analysis are shown in the Fig. 6. The initial data represent a symmetric profile $\phi(x, 0) = 1 - A_0 \operatorname{sech}^\alpha(x)$, $\phi_t(x, 0) = 0$, where α is a positive real parameter. Note that in the presence of the potential in Eq. (2.10) with $V_0 = \lambda(\lambda + 1)$ the above initial data exactly match the profile of the corresponding oscillational mode when $\alpha = \lambda$. In the absence of the potential, or in case of the repulsive potential, these initial data evolve into the oscillon solution.

The upper subplot of Fig. 6 shows the upper envelope of the oscillations of the field $\phi(0, t)$. The bottom subplot displays the basic frequency of the oscillations measured from the time period between two subsequent maxima. This observable is quite informative for identification almost periodic functions. However, in some situations the basic frequency cannot be easily identified in this way because of numerical artifacts. Thus we have also checked the results performing Fast Fourier Transform and generating the power spectrum of the data.

In Fig. 6 the black curve illustrates the evolution of the oscillational mode of the model (2.10) for a particular choice of the potential parameter $V_0 = 1.19$ ($\lambda = 0.7$). Initially this mode is excited up to nonlinear regime setting $A_0 = 0.6$. Due to the nonlinearity, the corresponding initial frequency ($\omega = 1.5$) is much lower initially than its value predicted from the linearized theory, $\omega_{osc} = 1.8735$. However, with time the energy is radiated away and the amplitude of oscillations slowly decays. Then the frequency raises and it

approaches the corresponding linearized value ω_{osc} . The decay rate of this mode follows the power law, $A \sim t^{-1/2}$ [1, 2].

The red curve shows the evolution of the oscillon configuration, which is produced from the similar initial data setting $A_0 = 0.7$ in the absence of the external potential, $V_0 = 0$. Note that both the amplitude and the frequency of the oscillations vary very slowly in comparison to the oscillational mode. Some small modulations of the frequency are still visible.

The blue curve shows the evolution of the oscillon initial data with $A_0 = 0.7$ as above, however, now in a presence of the repulsive potential, $V_0 = -0.39296$. As expected, for a given height of the potential only the oscillons with amplitude larger than some critical value can exist. Again, they slowly fade radiating energy away and we observe the decrease of the amplitude of the oscillations due to radiation loss. At some point the nonlinearities cannot hold together the oscillon which starts to oscillate with highly modulated amplitude (peaks of the blue line) just before it breaks in a short burst of radiation. This is the feature which has been observed for oscillons in higher dimensions as well [9].

For small positive values of V_0 it might happen that the oscillational mode would initially behave as oscillon (radiating very slowly) until the linear term $V_0(\phi - 1)$ becomes large enough in comparison to the nonlinear term $(\phi - 1)^2$. The smaller V_0 is the smaller the coupling between the oscillational mode and the second harmonic. The linear modes (attractors of the evolutions) become wider. The coefficient of proportionality multiplying the decay power law $t^{-1/2}$ becomes smaller. There is a smooth transition between oscillational modes $V_0 > 0$ and the oscillons $V_0 = 0$.

For $V_0 < 0$ the oscillon does not have a supporting mode and the potential is repulsive. There exists a certain amplitude below which the oscillon cannot exist as the nonlinearities have not enough strength to hold it together. In the evolution from the large amplitude at some point the oscillon loses its stability as the amplitude reaches the critical value. The oscillon rapidly vanishes into the radiation. Sometimes the radiation can have a form of two oscillons. In such a case the initial oscillon is literally torn apart by the potential into two smaller oscillons.

3.3 Adiabatic transformation

An interesting evolution scenario was observed for the situation when the initial data set rapidly converges to the oscillon configuration in the absence of the external potential (black curve in Figs. 7). Within the time interval $t \in [t_1, t_2]$ where $t_1 = 200$ and $t_2 = 400$ (yellow strip in Fig. 7), we gradually increase the depth of the potential as

$$V(t) = V_0 \frac{t - t_1}{t_2 - t_1}. \quad (3.1)$$

Here we set $V_0 = 1.19$ as above. Then the amplitude of the oscillations increases and, as $t > t_2$, the oscillating state becomes trapped by the potential well. Further, starting from this moment of time, the pattern of evolution of the configuration follows the usual $t^{-1/2}$ law of the radiative decay of the oscillational mode. In other words, the oscillon state becomes smoothly transformed into the oscillational mode.

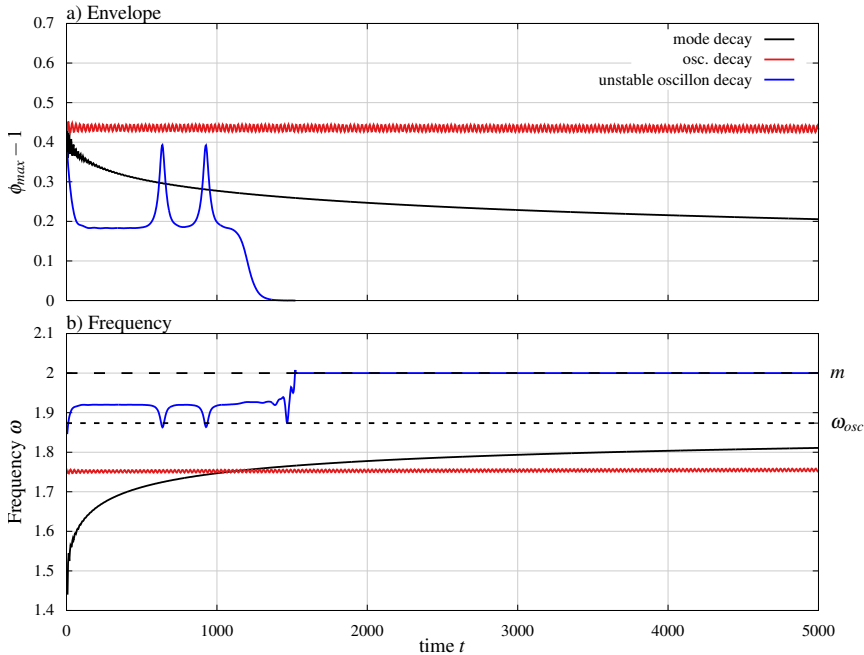


Figure 6. Possible relaxation scenarios for $A_0 = 0.6$. The plots show the maximum envelope of oscillations at $x = 0$ (upper plot) and the measured frequency as $\omega = 2\pi/T$ (bottom plot), where T is time between the subsequent maxima. Decay of the oscillational mode (black curve); usual evolution of the oscillon configuration (red curve); decay of the unstable oscillon in the repulsive potential (blue curve).

The opposite transition is illustrated in Fig. 7 by the red curves. Initially, there is an excited oscillational mode in the potential well with the same values of the parameters as above. As $t_1 < t < t_2$ the potential is turned off smoothly by setting

$$V(t) = V_0 \frac{t - t_2}{t_2 - t_1}, \quad (3.2)$$

and the oscillation mode becomes transformed into the oscillon state with amplitude a bit above $A = 0.2$ and the frequency $\omega = 1.9566$. This is clearly below the mass threshold. Both the frequency and the amplitude of the configuration are modulated by small oscillations, however, the corresponding average values are almost constant.

Finally, the blue curves in Fig. 7 show the decay of the internal mode in the potential with the initial depth $V_0 = 1.19$ as it changes adiabatically to $V_0 = -1$ as $t_1 < t < t_2$. During the change the oscillational mode turned into an oscillon which was destroyed by the repulsive potential as $V_0 < 0$.

3.4 Final state

Let us now consider dependency of the relaxation scenarios of the initial data on the parameters of the input configuration $\phi(x, 0) = 1 - A_0 \operatorname{sech}^\alpha(x)$, $\phi_t(x, 0) = 0$, as above. In Fig. 8 the upper plot shows the amplitude of the oscillations at $x = 0$ measured after

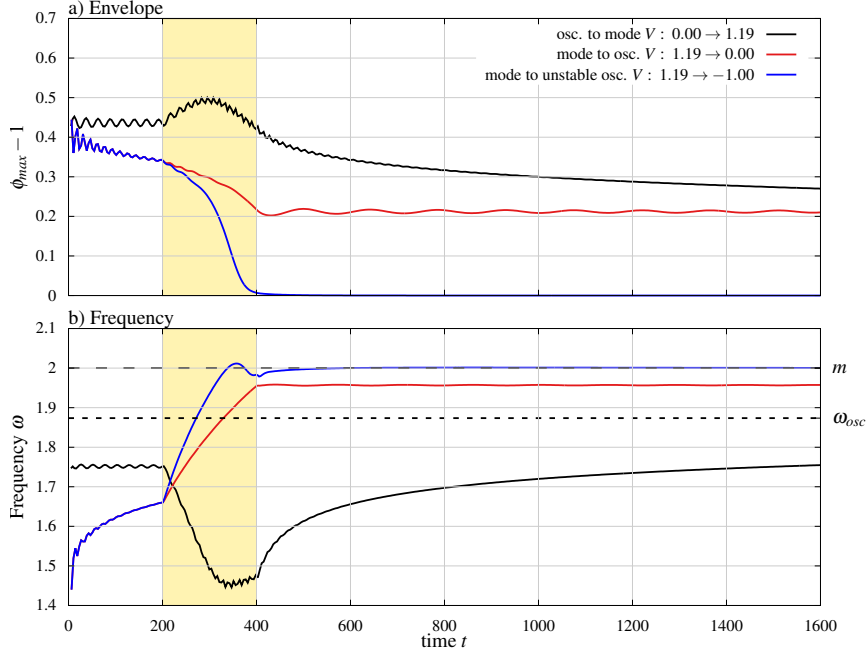


Figure 7. Examples of adiabatic transformations: (i) the oscillon $A_0 = 0.6$ to the internal oscillational mode (black curve); (ii) the oscillational mode to the oscillon (red curve); (iii) the oscillational mode to an unstable oscillon and its consequent decay (blue curve).

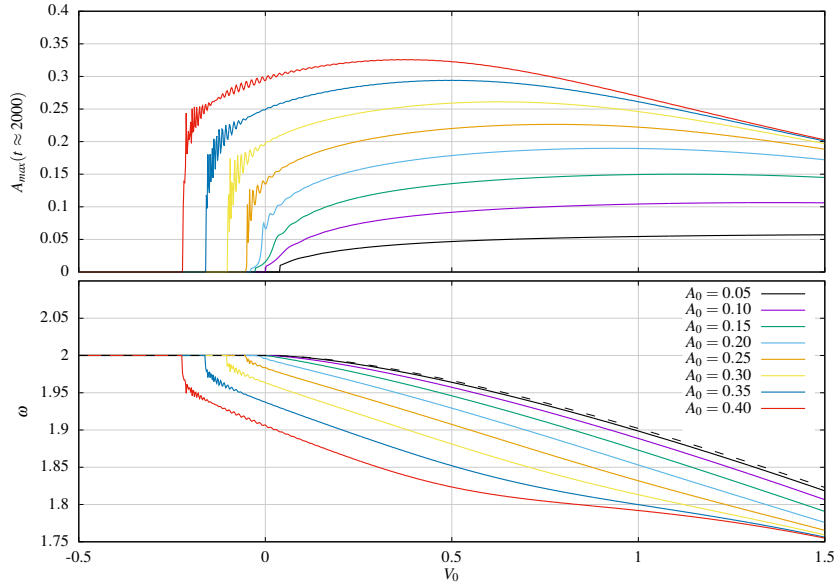


Figure 8. Upper plot: Amplitude measured after about $t = 2000$ from initial data with $\alpha = 0.4$ as a function of V_0 . Bottom plot: Measured frequency of the final state. The dashed line represents the frequency of the bounded mode of the corresponding potential at $A_0 = 0$.

time interval $t = 2000$ for different values of the initial amplitude A_0 as a function of the potential depth V_0 with $\alpha = 0.4$.

We observe, that for relatively small values of the initial amplitude, the oscillations above the vacuum are very small. This suggests that the system evolves following the linearized dynamics. The lower plot of Fig. 8 shows the measured frequency, which for small values of A_0 is very close to the frequency of the bounded mode of the corresponding linearized system. Thus, the initial perturbation can be decomposed into the linearized modes: one bounded mode and the modes from the continuum. The scattering modes move away from the center where only the oscillational mode remains. Note that as the initial amplitude increases, the frequency of the oscillations decreases.

Interestingly, there is a region $0 > V_0 > V_{cr}$, at which the final state is still oscillating, even in the case of the repulsive potential. Clearly, the corresponding frequencies are still below the mass threshold, although the repulsive potential does not support an oscillational mode.

In Fig. 8 one can see some modulations of the amplitude but, in general, there is no evidence of a clear distinction at the boundary $V_0 = 0$, both on the upper and on the lower plots.

It is usually assumed that whenever such persistent oscillations with the frequency below the mass threshold are seen in the absence of oscillational mode, an oscillon is produced from the initial data [8]. From the above simulations we can see that a distinction between an oscillon and an oscillational mode is quite artificial. The only difference is that the frequency of the oscillational modes tend to the frequency, calculated from the linearized model, as the amplitude decreases. In the case of oscillons, there is no mode, toward which they could approach, so they just slowly decay into the vacuum $V_0 = 0$, or until the repulsive potential with $V_0 < 0$ destroys the oscillon.

3.5 Phase diagram

In Fig. 9 we display a *phase diagram* indicating regions with different scenarios (basins of attraction) described above. The color scheme represents the minimal value of the field $\phi(0, t)$ at the center of the trapping potential for the time interval $80 < t < 100$ as function of the parameters α and V_0 . The dashed curve corresponds to the internal mode of the corresponding potential $V(x)$, $\alpha = \lambda$. Similar diagram, but now depending on the parameters A_0 and V_0 for fixed value $\alpha = 0.4$ is shown in Fig. 10.

Firstly, we observe that for negative values of the parameter V_0 , which correspond to region (II) colored in blue, the minimal value of the field approaches the vacuum. Physically, the corresponding initial oscillon configuration, which rapidly decays into the burst of radiation or a pair of smaller amplitude oscillons, see Fig. 11.

For sufficiently large value of the parameter α , which defines the width of the input data, and relatively small positive values of the parameter V_0 , we observed that the initial configuration evolves into slowly radiating oscillating mode, this scenario corresponds to the pink-white regions (I) in this plot. Note that as α becomes relatively small, the amplitude of the oscillations of the final state is increasing and the dynamics of the field turns out to be chaotic with multiple resonances related with production and annihilation of the

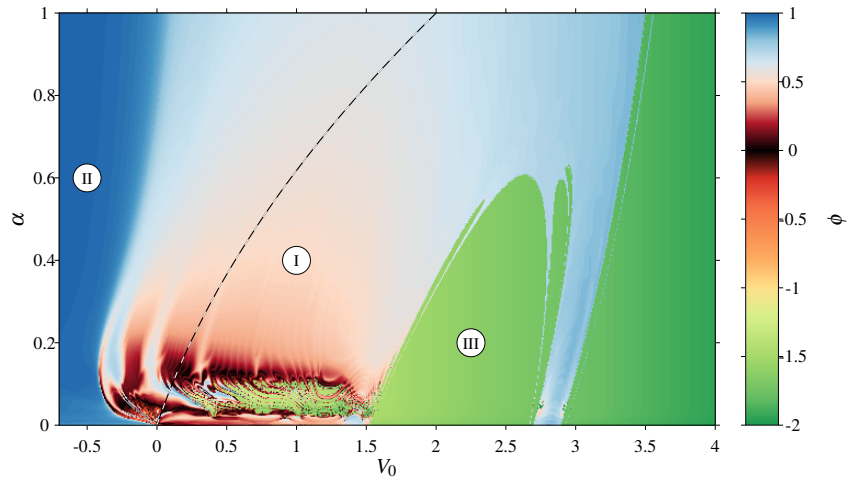


Figure 9. Minimal value of $\phi(0, t)$ for $80 < t < 100$ for $A_0 = 0.4$. The dashed curve corresponds to the parameters of the exact solution for the internal mode in the potential $V(x)$. White-red regions (I) correspond to oscillational mode (if $V_0 > 0$) and well developed stable oscillon (if $V_0 \leq 0$), dark blue (II) correspond to unstable oscillon, yellow-green (III) kink antikink creation.

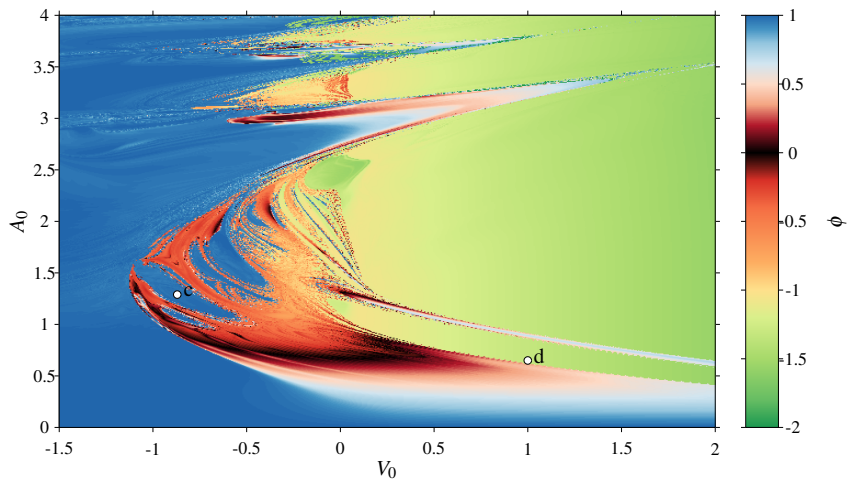


Figure 10. Minimal value of $\phi(0, t)$ for $\alpha = 0.4$.

kink–anti-kink pairs (region (III) see Fig. 12). On the other hand, this domain smoothly extends to the region, where $V_0 < 0$ and the internal mode ceases to exist. Thus, in such a case the final state represents an oscillon.

4 Conclusions

The main objective of this work is to demonstrate that there is an intrinsic relation between the oscillational normal modes and the oscillon configurations, which, under certain assumptions can be smoothly transformed into each other. As a simple example model we

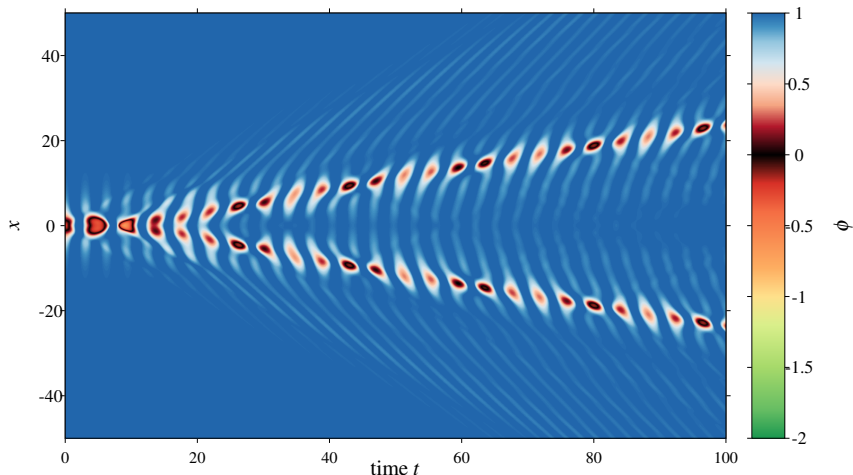


Figure 11. Unstable oscillon torn by the external potential into two oscillons ($V_0 = -0.81$, $A_0 = 1.32$).

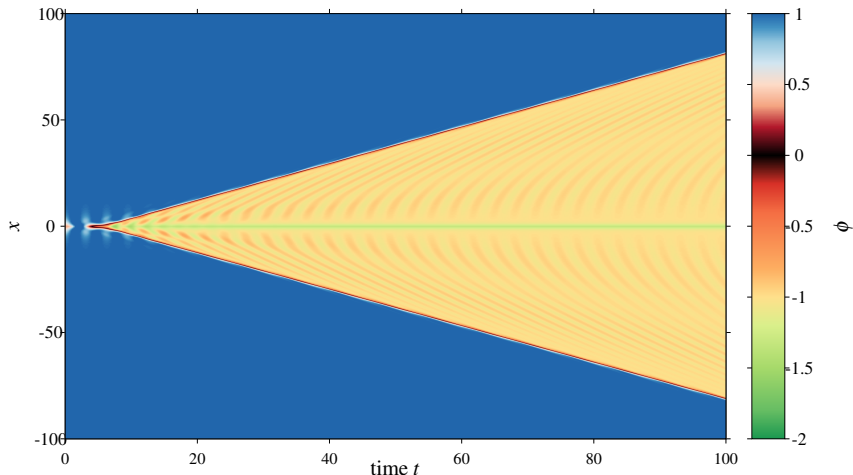


Figure 12. $K\bar{K}$ production ($V_0 = 1.06$, $A_0 = 0.69$).

considered a modification of the 1+1 dimensional ϕ^4 theory with a symmetric potential, which was used to introduce an external perturbation of the spectrum.

In our numerical experiment the potential was changed adiabatically from its attractive form, which supports an oscillational mode, to repulsive interaction. In the course of the evolution we observe the transformation of an oscillational mode into an oscillon configuration. In the opposite case, adiabatically switching the potential from repulsive to attractive form, we observe that an oscillon becomes smoothly transformed into an excited oscillational mode, which later starts to decay obeying the corresponding power law.

We also studied various evolution scenarios of a certain class of initial data. We found that, depending on the depth of the potential and the profile of the initial data, the

resulting configuration may represent either the oscillons or the oscillational mode. We also conjecture that the distinction between the oscillational mode and oscillon is rather artificial and in moderately long time dynamics there is no clear distinction between the two. In our phase diagrams we were unable to see any distinctive boundary separating oscillon from oscillational mode evolution types. Only extremely long time evolution could show the difference in the limiting case $V_0 \rightarrow 0$. Then the oscillational modes would vanish oscillating with the final frequency below the mass threshold and amplitude tending to zero while the oscillons either with frequency tending to the mass threshold and vanishing amplitude ($V_0 = 0$ case) or with some nonzero critical amplitude (repulsive $V_0 < 0$ case).

We did numerical simulation considering different values of the parameters of the potential b and V_0 , which corresponded to higher number of (even) bounded modes. In the most cases we observed that the lowest mode was an attractor in the time evolution of the initial data.

In the Appendix we studied the radiative decay of a single oscillational mode. We checked the validity of the Manton-Merabet approach, which leads to the power law decay of the mode, by direct measuring of the amplitude of the radiation, emitted by the excited mode. This approximation, however, fails in the case of deeper oscillational modes, in such a case higher harmonics are hidden below the mass threshold and the mode decays much slower than it is predicted by the Manton-Merabet law [3]. One of the most interesting findings we examined in this paper is the observation of burst or radiation, which happens as the slowly decreasing frequency of higher harmonic of the initially highly excited oscillational mode, crosses the mass threshold and starts to propagate. This feature may be important in other nonlinear field theories, which may support deeper oscillational modes, for example in the Skyrme model [22].

Another important observation is that as the potential vanishes, the frequency of the oscillational mode tends to the frequency of the mass threshold from below. Moreover, the radiation amplitude calculated from the second order perturbative scheme also vanishes along with the potential. This yields yet another illustration of smooth character of the transition from the oscillational mode to the oscillon in the parametric space.

Our observations could indicate that similar scenario is also possible in higher dimensional field theoretical systems. In principle one does not need to limit the considerations to the external potential. Topological defects or solitons can be the source of a very similar potential as examined in the current paper. Both oscillons and the bound modes of the solitons were studied extensively in the past. However, an open question remains whether a configuration of a topological defect bound with an oscillon can exist.

Another question, which we hope to be addressing in the near future, is to consider the dynamics of the kinks in the presence of the localizing potential. It will extend the related analysis of the dynamics of the solitons with delta-like inhomogeneity [16–18].

Acknowledgements: The authors are grateful to Patrick Dorey for inspiring and valuable discussions and Boris Malomed for his valuable comments and correspondence. YS gratefully acknowledges support from the Russian Foundation for Basic Research (Grant No. 16-52-12012), the Ministry of Education and Science of Russian Federation, project No 3.1386.2017, and DFG (Grant LE 838/12-2). YS would like to thank the Institute of

Physics, Jagiellonian University, Krakow for its kind hospitality.

A Time evolution of the oscillational mode

A.1 Manton-Merabet power law

Let us assume that a mode around the trivial vacuum $\phi = 1$ is excited. The linear analysis gives us the frequency of its small amplitude oscillations, it corresponds to the solution of the Eq. (2.11). In nonlinear theories, large amplitude excitations can change the fundamental frequency of the oscillations. Oscillational modes are unstable, they radiate due to the coupling to the modes of continuum, so the frequency of oscillations and the amplitude of the mode A evolve with time, the amplitude of the oscillations will slowly decrease while the corresponding frequency (usually) will increase towards the value obtained from the linearization.

In a similar consideration of the time evolution of the internal oscillational mode of the usual ϕ^4 kink, Manton and Merabet showed that this mode decays due to the radiation following the rule $A \sim t^{-1/2}$ [1]. Their arguments can be summarized as follows. The evolution of the mode can be described via a perturbative expansion in the powers of the amplitude

$$\phi = 1 + \sum_{n=1} A^n \xi^{(n)}. \quad (\text{A.1})$$

Substituting this expansion into the linearized field equation for fluctuations, we can see that each term of the perturbation series should satisfy the equation of the form:

$$\xi_{tt}^{(n)} + \mathbf{L}\xi = g^{(n)}(\xi^{(1)}, \dots, \xi^{(n-1)}), \quad (\text{A.2})$$

where

$$\mathbf{L} = -\partial_x^2 + m^2 + V(x), \quad (\text{A.3})$$

is a linear operator and

$$g^{(n)}(\xi^{(1)}, \dots, \xi^{(n-1)}), \quad (\text{A.4})$$

is a source term which depends only on the solutions of the lower order.

For example in the first two orders we obtain

$$g^{(1)} = 0, \quad g^{(2)} = -6\xi^{(1)2} \quad (\text{A.5})$$

Note that in the second order the source term is given by the square of the solution of the first order equation. If the time dependence of the fluctuations in the first order is harmonic, i.e. $\xi^{(1)} \sim \cos\omega t$, the source term oscillates like $g^{(2)} \sim 1 + \cos(2\omega t)$. This is a source of radiation with a frequency 2ω , which carries away the energy from the mode causing its decay.

Note that the amplitude of the radiation in the lowest order is proportional to A^2 , thus the energy flow is $dE/dt \sim A^4$. Further, since the energy of the oscillational mode is proportional to A^2 the decay of the mode should follow the power law

$$\frac{dA}{dt} \sim -A^3 \Rightarrow A(t) \sim t^{-1/2}. \quad (\text{A.6})$$

Here the proportionality coefficient can be found using Green function technique and expressed as an integral over a function of eigenfunctions of the corresponding linearized problem:

$$\xi^{(2)}(x \rightarrow \infty) \approx \frac{3e^{2i\omega t}\eta_{-k}(x)}{2W} \int_{-\infty}^{\infty} \eta_0(x')^2 \eta_k(x') dx' + c.c \equiv \mathcal{A} \cos(2\omega t - kx + \delta). \quad (\text{A.7})$$

where $W = \eta_k \eta'_{-k} - \eta'_k \eta_{-k}$ is a Wronskian and $k = \sqrt{4\omega^2 - m^2}$ is the wave number for the second harmonic, \mathcal{A} is the amplitude of the radiation and δ is some phase shift.

In general, the eigenfunctions of the Pöschl-Teller potential can be expressed in terms of Legendre polynomials

$$\eta_k(x) = P_{\lambda}^{ik}(\tanh x), \quad k = \sqrt{k^2 - m^2}, \quad (\text{A.8})$$

however, the corresponding integrals in (A.7) can be calculated analytically only for certain values of λ . As $\lambda \rightarrow 0$ (or $V_0 \rightarrow 0$) the amplitude of the second harmonic also vanishes. This is yet another similarity with the oscillons. In [21] it was shown that oscillons radiate beyond all orders, meaning that the radiation amplitude cannot be represented as a simple power series and that all coefficients of the perturbation series are equal zero.

A.2 Numerical verification

We have calculated the amplitude numerically and compared it with the measurements performed for small values of amplitude A of the oscillational mode (Figure 13). The amplitude was measured at the distance $x = 200$ at the time $t = 1000$. The amplitude obtained from evolution is in good agreement with the second order calculations for $1.5 < V_0 < 4.6$. Below the lower value the amplitude of the second harmonic is small and comparable with other types of radiation. Below $V_0 = 1$ the discrepancy is significant but the scaling $\mathcal{A} \sim A^2$ seems to be preserved. This could mean that either our predicted amplitude is wrong or other modes dominate. In our simulations we started the evolution with initial conditions corresponding to the excitation of the pure oscillational mode at a given time $t = 0$. The source term $g^{(2)}$ is then not entirely harmonic (with a single frequency). It should be multiplied by a Heaviside step function³. This means that all the frequencies ($\mathcal{F}[H(t)e^{i\omega_0 t}] = \frac{1}{2}\delta(\omega - \omega_0) - \frac{i}{2\pi(\omega - \omega_0)}$) contribute to the evolution and a single frequency approximation fails. As the result, the radiation amplitude consists of not only the amplitude of the second harmonic (A.7) but is a sum/integral of amplitudes of all the modes. This should be especially visible when the second harmonic amplitude tends to 0 as $V_0 \rightarrow 0$.

In order to verify the above predictions we have plotted a power spectra of the field measured at the center ($x = 0$) and far away ($x = 200$) from the center for initially excited $A = 0.01$ oscillational mode for a few values of V_0 (Figure 14). For $V_0 = 2$ (a) the most dominating frequency in the far field measurements is $2\omega_1$. The height of a peak is not much lower than the predicted $\mathcal{A}A^2 = 5.2 \cdot 10^{-6}$. For $V_0 = 0.5$ (b) the height for the second harmonic is also close to the predicted value of $4.2 \cdot 10^{-7}$ but it is not the most dominating

³more precise analysis of this problem in the case of excited ϕ^4 kink can be found in [23]

frequency now. The spectrum is highly contaminated with the frequencies near the mass threshold $\omega \approx m = 2$. So that means that indeed the radiation amplitude is proportional to the square of the amplitude of the oscillational mode, but for $V_0 \rightarrow 0$ the second harmonic is not the most dominating frequency in the spectrum.

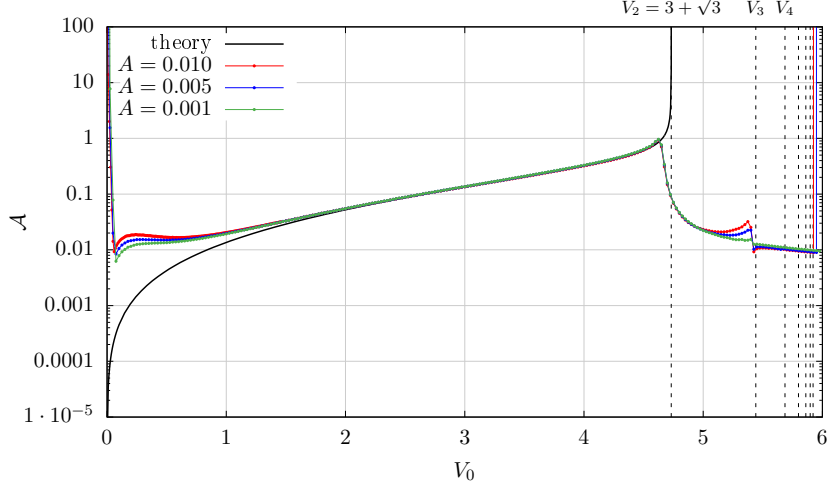


Figure 13. Radiation measured at $x = 200$ at $t = 1000$ (divided by A^2) compared with the theoretically predicted values (A.7) (black curve).

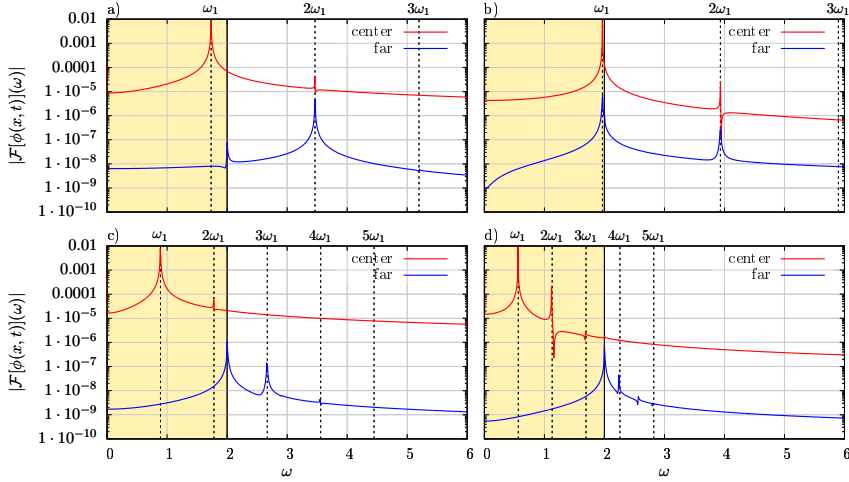


Figure 14. Power spectra of the measured at the center $x = 0$ (red) and far $x = 200$ field (blue) for different values of the potential depth V_0 and for initial excitation of the oscillational mode $A = 0.01$. Four different scenarios correspond to a) $V_0 = 2.0$ - almost pure second harmonic, b) $V_0 = 0.5$ - large contamination of the near-the-threshold modes, c) $V_0 = 5.0$ - decay through the third harmonic, d) $V_0 = 5.6$ - decay through the fourth harmonic.

A.3 Deep modes relaxation

Note that the above consideration is valid only when two following conjectures are fulfilled. First, we consider the amplitude of oscillations to be small enough to secure the convergency of the perturbation series in A . Another assumption is that the second harmonic belongs to the continuous scattering spectrum. This second conjecture, however, is true only when the potential is not too deep so that

$$b^2\lambda^2 < \frac{3m^2}{4}, \quad (\text{A.9})$$

or, in other terms:

$$V_0 < \frac{3m^2}{4} + \frac{m\sqrt{3}}{2}b. \quad (\text{A.10})$$

If this condition is not fulfilled, the second harmonic remains below the mass threshold and cannot propagate. This happens for $V_0 > V_2 = \sqrt{3} + 3$ (for $b = 1$, $m = 2$). For $V_0 = V_2$ the integral in (A.7) is divergent (Figure 13). For $V_0 > V_2$ the approximation (A.7) is not valid. Numerical simulations show that even for some range below V_2 the perturbation approach fails. This corresponds to the case when the frequency of the second harmonic is very close to the mass threshold ($2\omega_1$ is almost in a resonance with m).

In order to calculate the energy loss of the oscillational mode for $V_0 > V_2$, one has to include the higher order terms of perturbation series in consideration. Assuming that the third harmonic is the first one, which can propagate, we can expect that the decay rate of the mode becomes

$$A(t) \sim t^{-1/4}. \quad (\text{A.11})$$

However, as the potential depth is increasing, more and more higher harmonics move down below the mass threshold. This happens as

$$\lambda_n = \frac{m}{nb} \sqrt{n^2 - 1}, \quad V_n = \lambda_n b^2 (\lambda_n^2 - 1), \quad (\text{A.12})$$

where $n \geq 2$ is the number of the first propagating harmonic. It yields the generalized power decay law of the oscillational mode

$$A(t) \sim t^{-\frac{1}{2n-2}}. \quad (\text{A.13})$$

This feature was first pointed out in [3]. Power spectra exemplifying the radiation through the third and fourth harmonics are shown in the Figure 14 c) and d) respectively.

Note that in the consideration above we assume that the amplitude of the mode A is small enough, so the higher order corrections do not contribute much.

The nonlinearities can act at least in two ways. One is the appearance of that higher harmonics as considered earlier. The other effect is that the measured frequency $\omega(A)$ is lower than the eigenfrequency ω_1 obtained from the linear analysis, usually: $\omega(A) = \omega_1 - c_2 A^2 + \dots$, with $c_2 > 0$. In the classical mechanics this effect can be seen in the case of pendulum or anharmonic oscillator. Let us consider a mode with ω_1 just above $m/2$. When the mode is largely excited, it may happen that $\omega(A) < m/2$. In this scenario, the radiative decay would occur in two stages. Initially the second harmonic with the frequency

$2\omega(A) < m$ cannot propagate. The mode decays slowly through the third harmonic. As the amplitude decreases, the frequency $\omega(A)$ grows and, for certain amplitude, crosses $m/2$, allowing the second harmonic to propagate. As the result the relaxation process accelerates. At some distance this transition can be seen as a sudden burst of radiation.

In Fig. 15 we show different scenarios of decays of the oscillational mode. In our numerical simulations we set $b = 1$ and we suppose that the potential depth is restricted by the inequality (A.10), i.e. $V_0 \lesssim V_2 = 3 + \sqrt{3} \approx 4.7321$. Thus, in the (close to) linear regime, $A \rightarrow 0$, the first harmonic is initially bounded, while the second harmonic can propagate.

The initial data were taken according to (2.11) as

$$\phi(x, 0) = 1 + \frac{A_0}{\cosh^\lambda(bx)}, \quad \phi_t(x, 0) = 0. \quad (\text{A.14})$$

The value of the initial amplitude $A_0 = 0.08$ is just enough to lower the frequencies of the oscillational modes below the second frequency threshold $\omega(A_0, V_0) < m/2 = 1$ for $V_0 \geq 4.5770$. The relaxation of these modes is much slower than the relaxation of the modes, for which the frequency is above the threshold $\omega(A_0, V_0) > m/2$ for $V_0 < 4.5770$.

In Fig. 15 we also show an example of the transition between two different types of the decay, when initially the frequency was set below $m/2$ but in time the sufficient amount of energy was radiated so that the frequency would increase above the threshold $m/2$ releasing the second harmonics. As the result the energy loss of the oscillational mode due to its radiative decay increased dramatically.

Note that for the field of the decaying oscillating state (the purple and orange curves in the Fig. 15) for $t > 1000$ can be nicely fitted by the function

$$\phi(0, t) = 1 + a(t - t_0)^c \quad (\text{A.15})$$

where in both cases $c = -0.478$. Thus, the prediction of the power law decay is correct.

References

- [1] N. S. Manton and H. Merabet, ϕ^4 kinks: Gradient flow and dynamics, *Nonlinearity* **10** (1997) 3, [[hep-th/9605038](#)].
- [2] M. Slusarczyk, Dynamics of a planar domain wall with oscillating thickness in $\lambda\phi^4$ model, *Acta Phys. Polon.* **B31** (2000) 617–635, [[hep-th/9903185](#)].
- [3] P. Dorey, A. Halavanau, J. Mercer, T. Romańczukiewicz and Y. Shnir, Boundary scattering in the ϕ^4 model, *JHEP* **05** (2017) 107, [[1508.02329](#)].
- [4] P. Bizon, T. Chmaj and N. Szpak, Dynamics near the threshold for blowup in the one-dimensional focusing nonlinear Klein-Gordon equation, *J. Math. Phys.* **52** (2011) 103703.
- [5] H. Arodz, P. Klimas and T. Tyranowski, Compact oscillons in the signum-Gordon model, *Phys. Rev.* **D77** (2008) 047701, [[0710.2244](#)].
- [6] G. Fodor, P. Forgacs, Z. Horvath and M. Mezei, Computation of the radiation amplitude of oscillons, *Phys. Rev.* **D79** (2009) 065002, [[0812.1919](#)].

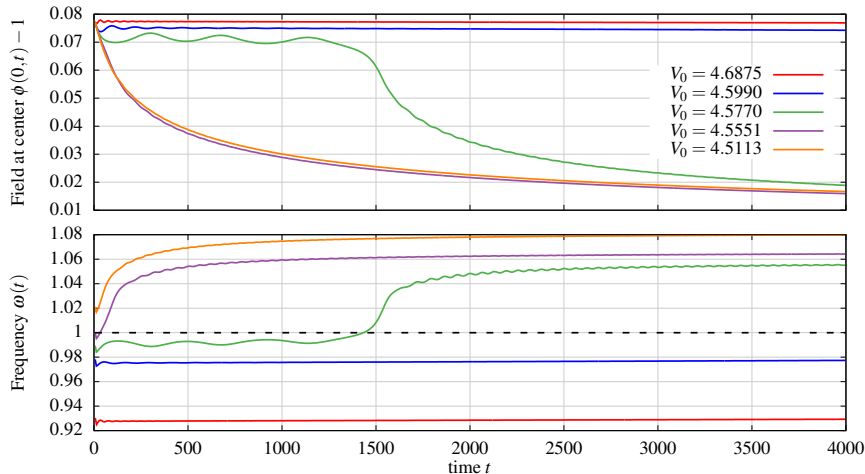


Figure 15. Time evolution of the oscillational mode with amplitude $A_0 = 0.08$ potential width $b = 1$ and various depths just below the value when the second harmonics is hidden in the linear approximation. Upper plot shows the maxima of field value at $x = 0$, the bottom plot shows the measured frequency $\omega(t) = 2\pi/T$, where T is a time between two subsequent maxima. The red and blue curve represent slow relaxation through the third harmonic, the green curve shows the transition between two different types of decay, which appear due to the nonlinearities related with relatively large values of the amplitude, the purple and orange curves correspond to the radiative decay through the propagation of the second harmonics.

- [7] I. L. Bogolyubsky and V. G. Makhankov, *On the Pulsed Soliton Lifetime in Two Classical Relativistic Theory Models*, *JETP Lett.* **24** (1976) 12.
- [8] E. J. Copeland, M. Gleiser and H. R. Muller, *Oscillons: Resonant configurations during bubble collapse*, *Phys. Rev.* **D52** (1995) 1920–1933, [[hep-ph/9503217](#)].
- [9] M. Gleiser, *Pseudostable bubbles*, *Phys. Rev.* **D49** (1994) 2978–2981, [[hep-ph/9308279](#)].
- [10] G. Fodor, P. Forgacs, P. Grandclement and I. Racz, *Oscillons and Quasi-breathers in the ϕ^4 Klein-Gordon model*, *Phys. Rev.* **D74** (2006) 124003, [[hep-th/0609023](#)].
- [11] P. Salmi and M. Hindmarsh, *Radiation and Relaxation of Oscillons*, *Phys. Rev.* **D85** (2012) 085033, [[1201.1934](#)].
- [12] D. K. Campbell, J. F. Schonfeld and C. A. Wingate, *Resonance structure in kink-antikink interactions in ϕ^4 theory*, *Physica D: Nonlinear Phenomena* **9** (1983) 1 – 32.
- [13] P. Anninos, S. Oliveira and R. A. Matzner, *Fractal structure in the scalar $\lambda(\phi^2 - 1)^2$ theory*, *Phys. Rev.* **D44** (1991) 1147–1160.
- [14] T. Romanczukiewicz, *Creation of kink and antikink pairs forced by radiation*, *J. Phys.* **A39** (2006) 3479, [[hep-th/0501066](#)].
- [15] T. Romanczukiewicz and Ya. Shnir, *Oscillon resonances and creation of kinks in particle collisions*, *Phys. Rev. Lett.* **105** (2010) 081601, [[1002.4484](#)].
- [16] Z. Fei, Y. S. Kivshar and L. Vázquez, *Resonant kink-impurity interactions in the φ^4 model*, *Phys. Rev. A* **46** (Oct, 1992) 5214–5220.

- [17] M. I. W. Roy H Goodman, Philip J Holmes, *Interaction of sine-Gordon kinks with defects: phase space transport in a two-mode model*, *Physica D* **161** (2002) 21–44.
- [18] Y. S. Kivshar, Z. Fei and L. Vázquez, *Resonant soliton-impurity interactions*, *Phys. Rev. Lett.* **67** (Sep, 1991) 1177–1180.
- [19] R. Rajaraman, *Solitons of Coupled Scalar Field Theories in Two-dimensions*, *Phys. Rev. Lett.* **42** (1979) 200.
- [20] A. Halavanau, T. Romańczukiewicz and Ya. Shnir, *Resonance structures in coupled two-component ϕ^4 model*, *Phys. Rev.* **D86** (2012) 085027, [[1206.4471](#)].
- [21] J. P. Boyd, *Weakly nonlocal envelope solitary waves: numerical calculations for the klein-gordon (ϕ^4) equation*, *Wave Motion* **21** (1995) 311 – 330.
- [22] C. Adam, M. Haberichter, T. Romanczukiewicz and A. Wereszczynski, *Roper resonances and quasi-normal modes of Skyrmions*, [1710.00837](#).
- [23] T. Romańczukiewicz, *Interaction between kink and radiation in ϕ^4 model*, *Acta Phys. Polon.* **B35** (2004) 523–540, [[hep-th/0303058](#)].